Mitochondrion 56 (2021) 82–90

Contents lists available at ScienceDirect

Mitochondrion

journal homepage: www.elsevier.com/locate/mito

Ultraviolet irradiation alters the density of inner mitochondrial membrane and proportion of inter-mitochondrial junctions in copepod myocytes

Kyle B. Heine *, Nicholas M. Justyn, Geoffrey E. Hill, Wendy R. Hood

Department of Biological Sciences, Auburn University, Auburn, AL 36849, USA

ARTICLE INFO

Keywords:
Fission
Metabolic rate
Mitochondrial behavior
Morphology
Tigriopus californicus
Transmission electron microscopy

ABSTRACT

The efficient production of energy via oxidative phosphorylation is essential to the growth, survival, and reproduction of eukaryotes. The behavior (position of, and communication between, mitochondria) and morphology of mitochondria play key roles in efficient energy production and are influenced by oxidative stressors such as ultraviolet (UV) radiation. We tested the hypothesis that mitochondria change their behavior and morphology to meet energetic demands of responding to changes in oxidative stress. Specifically, we predicted that UV irradiation would increase the density of inner mitochondrial membrane and proportion of inter-mitochondrial junctions to influence whole-animal metabolic rate. Using transmission electron microscopy, we found that both three and six hours of UV-A/B irradiation (0.5 W/m^2) increased the proportion of inter-mitochondrial junctions (with increasing mitochondrial aspect ratio) and the density of inner mitochondrial membrane in myocytes of *Tigriopus californicus* copepods. Mitochondrial density increased following both irradiation treatments, but mitochondrial size decreased under the six hour treatment. Metabolic rate was maintained under three hours of irradiation but decreased following six hours of exposure. These observations demonstrate that the density of inner mitochondrial membrane and proportion of inter-mitochondrial junctions can play formative roles in maintaining whole-animal metabolic rate, and ultimately organismal performance, under exposure to an oxidative stressor.

1. Introduction

Explaining variation in whole-animal performance, which we define as the capacity to produce sufficient adenosine triphosphate (ATP) to support growth, self-maintenance, and reproduction, is a central goal of functional and physiological ecology (e.g., Drent and Daan, 1980; Kenagy et al., 1990; Salin et al., 2019; Speakman et al., 2015). For complex animals, 90% of ATP is produced via oxidative phosphorylation in mitochondria, so the efficiency of the electron transport system (ETS) is a key determinant of energy production for most animals (Hill, 2019). In addition to ETS function, the behavior (position and communication within the cell) and morphology of mitochondria are also proposed to play key roles in the capacity of energy production (Heine and Hood, 2020). Past research has been successful in explaining how mitochondrial behavior and morphology impact the ability of mitochondria to produce energy efficiently (Mannella et al., 2013; Zick et al., 2009), as well as in characterizing variation in whole-animal performance (e.g., Speakman and Król, 2005). However, support for different hypotheses for how changes in mitochondrial behavior and structure impact animal performance (including stress responses) as a whole are equivocal.

Documented changes in the behavior and morphology of mitochondria suggest that they likely play formative roles in the energetic capacity of tissues. The density of inner mitochondrial membrane (IMM), proportion of inter-mitochondrial junctions (IMJs), and mitochondrial density have all been shown to increase with increased energetic demand. Moreover, the rates of mitochondrial fission and fusion will vary in relation to mitochondrial damage and dysfunction caused by an increase in the production of free radicals such as superoxide or hydroxyl radicals (*see* Heine and Hood, 2020 *for a review*). The IMM contains protein complexes I-IV of the ETS that create an electrochemical gradient across the IMM, driving the production of ATP at complex V. Protons are actively pumped from the mitochondrial matrix into the inter-membrane space by complexes I, III, and IV, as complexes I and II deliver electrons to the quinone pool, and complex IV reduces oxygen to water. Protons flow down the electrochemical gradient through complex V to form ATP (Hatefi, 1985). A greater density of IMM can support more complexes of the ETS, leading to greater ATP production under increased energetic demand (Nielsen et al., 2017; Strohm

* Corresponding author.
E-mail address: kbh0039@auburn.edu (K.B. Heine).

https://doi.org/10.1016/j.mito.2020.11.001
Received 8 June 2020; Received in revised form 18 October 2020; Accepted 2 November 2020
Available online 19 November 2020

and Daniels, 2003). IMJs are electron-dense contacts between mitochondria. IMJs are more common in tissues with higher energetic demand, such as heart muscle (Picard et al., 2015), and become more numerous when animals participate in energetically demanding behaviors such as running (Picard et al., 2013a). Although the proximate function of these structures remains to be confirmed through empirical research, they have been proposed to facilitate the coordination of gene expression, as in bacteria (Ng and Bassler, 2009), and/or the transfer of electrochemical gradients (*see* Pacher and Hajnoczky, 2001; Santo-Domingo et al., 2013). In turn, these changes may increase ATP production under increased energetic demand. Lastly, an increase in mitochondrial density in cells may increase the energetic capacity of organs (Hood et al., 2019), irrespective of changes in mitochondrial morphology.

Several exogenous stressors, including ultraviolet (UV) radiation, are known to influence mitochondrial performance. UV-B radiation can produce reactive oxygen species (ROS) through interactions with cellular catalase (Heck et al., 2003). In turn, ROS can impact cellular performance in both negative and positive ways, including damaging the cell (Finkel and Holbrook, 2000) or acting as signaling molecules to increase mitochondrial performance through the upregulation of antioxidants, mitochondrial biogenesis, or repair enzymes (Hood et al., 2018; Zhang et al., 2018). In addition to producing ROS, UV radiation can damage DNA directly (Cadet et al., 2005). The impact of UV radiation on performance is particularly relevant for organisms that must energetically respond to variable levels of direct sunlight, including invertebrates that inhabit marine environments. Previous work has shown that UV radiation can both impact mitochondria (Han et al., 2016) and increase reproductive performance in copepods (Heine et al., 2019; Hylander et al., 2014). Such energetically demanding changes to whole-animal performance likely stem from changes in mitochondrial function, which could be mediated, in part, by changes in mitochondrial behavior and morphology. *Tigriopus californicus* copepods are an ideal model to study how radiation impacts mitochondrial structure and metabolic rate because this species lives in shallow splash pools and is exposed to varying levels of UV irradiation throughout any given day (Weaver et al., 2018). Furthering our understanding of how UV irradiation impacts the behavior and morphology of mitochondria, and metabolic rate, allows us to better understand how pervasive organisms such as copepods are able to function in such variable environments. Accordingly, this study sought to address the links between mitochondrial behavior, morphology, and animal performance in copepods, as mediated by UV irradiation.

We tested the hypothesis that UV irradiation influences: 1) whole-animal metabolic rate and 2) mitochondrial behavior and morphology—specifically the density of IMM and proportion of IMJs in myocytes of the copepod *T. californicus*. Copepods were exposed to zero, three, or six hours of UV-A/B irradiation (0.5 W/m^2), after which we recorded the metabolic rate of each copepod for one hour. Transmission electron microscopy (TEM) was completed on a subset of these individuals to quantify mitochondrial behavior and morphology. We predicted that UV irradiation would increase the density of IMM and proportion of IMJs since these traits have been linked to increased energetic demand. We also quantified mitochondrial area and density to assess any changes in mitochondrial fission or fusion, as well as mitochondrial aspect ratio (*see* Leduc-Gaudet et al., 2015) which may impact mitochondrial performance.

2. Materials and methods

2.1. Copepod husbandry

This study was conducted from March to November 2019. All *Tigriopus californicus* copepods were acquired from Reef Nutrition, Campbell, CA in December 2018. Panmictic cultures of copepods were housed in 739 mL containers and were kept on a natural, ambient light cycle from laboratory windows at 20–22 °C. All cultures were fed ad libitum *Isochrysis galbana* algae in artificial sea water of salinity S = 32.

2.2. Data collection

Male *T. californicus* copepods clasp virgin females until the female becomes sexually mature after completing her final copepodid molt; the male then inseminates the female and releases her (Burton, 1985). Mating pairs were collected from our cultures and placed into 60 × 15 mm petri dishes half-filled with artificial sea water of salinity S = 32 and ad libitum *I. galbana* algae. Males were removed from petri dishes and placed back into cultures once the male inseminated and released the female. Females were placed back into cultures once her first clutch hatched. Offspring of the first clutch (n = 15 controls from two mothers, 18 individuals from three mothers in the 3-hr UV treatment, and 19 individuals from one mother in the 6-hr UV treatment) were raised to 22 ± 3 days before irradiation treatments. These numbers of mothers and offspring were chosen to age-match the offspring as closely as possible to avoid any possible age-related effects in our study.

For irradiation treatments, each copepod was placed into a well of a 24-well plate half-filled with artificial sea water of salinity S = 32. The plate was placed inside a black bin with either a full-spectrum light (Exo Terra Full Spectrum Natural Daylight Bulb; produces no UV-B; placed so that animals were exposed to no UV-A) or a UV-A/B light (Exo Terra 10.0 UVB Repti Glo Desert Terrarium Lamp; wavelengths ≥ 290 nm) suspended above the bin. Both the lamps and bin were covered with a black drape to remove any effects of ambient lighting. For each set of animals, the UV lamp was secured approximately 0.5 m above the bottom of the bin. A Sper Scientific UV-A/B light meter was placed in the bin, and then the distance between the light and the meter was adjusted until the meter measured 0.5 W/m^2. The light meter was then replaced with the plate of copepods. All copepods were assigned to one of three treatments: a 1-hr control treatment, or a 3- or 6-hr UV irradiation treatment. The 1-hr control and 3-hr UV irradiation treatments were chosen based on previous work that showed an increase in size of the first clutch following the same 1-hr control and 3-hr UV irradiation treatments (Heine et al., 2019; *see also* Han et al., 2016). The 6-hr UV irradiation treatment was chosen to represent a higher dose of radiation than the 3-hr treatment which, we have previously shown, increases reproductive performance in copepods (Heine et al., 2019); the impacts of the 6-hr treatment on reproductive performance are unknown.

2.3. Metabolic rate

Immediately following irradiation, each copepod was placed inside an 80 μL well of a 24-well fiber optics respirometer (PreSens, SDR SensorDish Reader, Loligo Systems) in the absence of food. We recorded change in dissolved oxygen for each copepod during one hour after a ~30-minute acclimation period. All assays were completed in autoclaved artificial sea water of S = 32 at 23 °C room temperature. Metabolic rate (R) was calculated as:

$$R = |[[\ (\mathrm{DO})_{t2} - (\mathrm{DO})_{t1}]/\Delta t]/\mathrm{L}|$$

where DO is dissolved oxygen in mmol/L, t is time in seconds (measured in 15 s increments), and L is body length (measured in mm). Measurements (and corresponding copepods) that did not yield a decrease in DO over time were excluded from the study (n = five controls, zero 3-hr UV treatments, and one 6-hr UV treatment); this is likely due to trapped air in the bottom of the well of the respirometer that was not seen by the operator, or an insufficient seal. Copepods were placed into primary fixative immediately following respiration assays. Once deceased, each copepod was photographed on a 1 × 1 mm grid under a dissecting microscope in the absence of fixative, and the length (mm) of each copepod was calculated as the distance from the center of the eyespot to the branch in the urosome. Length measurements were completed in ImageJ

(Rueden et al., 2017). After each copepod was photographed, the distal half of the urosome was removed to allow for the infiltration of fixative, and the copepod was placed back into primary fixative in a 3.5 mL glass vial and stored overnight at 4 °C.

2.4. Transmission electron microscopy

Primary fixative was prepared at a final concentration of 12.5 mL of 0.2 M phosphate buffer, 6.25 mL of 10% glutaraldehyde, 5 mL of 10% formaldehyde, and 1.25 mL dH_2O. Tissue was washed for 30 min with 0.1 M phosphate buffer three times then placed into a secondary fixative of 2% osmium tetroxide in the dark at room temperature for one and a half hours. Tissue was then dehydrated through a seven-step series from 30, 50, 70, 80, to 90% EtOH at 30 min each, followed by two 45-minute washes in 95% EtOH, and two one-hour washes in 100% EtOH. Samples were then placed into a transitional solvent of propylene oxide (PO) for two 30-minute washes. Tissue was then infiltrated with a PO/Epon resin mixture at a 2:1 ratio for three days, a 1:1 ratio for three days, a 1:2 ratio for three days, and lastly, pure resin for an additional three days. Expanding our infiltration to 12 days was the only means by which we obtained intact, well-preserved tissue (*see* Hopkins, 1978). Each copepod was embedded longitudinally in pure Epon resin and cured at 70 °C for 24 h. Ultra-thin, 80 nm longitudinal sections (cutting approximately one-fourth into the copepod to sample muscle tissue along the lateral surface of the prosome) of samples were ultra-microtomed and placed onto 200 mesh copper grids. Sections were then stained with uranyl acetate and lead citrate to increase contrast.

We then performed TEM using a ZEISS EM10 transmission electron microscope. We imaged, at random, three myocytes from the prosome of each copepod. For each myocyte, we collected one image at ×8,000 to quantify mitochondrial density and the proportion of IMJs, and three images at a magnification of ×25,000 to quantify mitochondrial aspect ratio, area, and the density of IMM. Measurements at ×25,000 were completed only on mitochondria from which we could distinguish both inner and outer membrane. All images and measurements were completed only for mitochondria within the subsarcolemmal space of each myocyte (i.e., between the cell membrane and myofibrils).

2.5. Mitochondrial behavior and morphology measurements

All mitochondrial behavior and morphology measurements were completed using ImageJ. Measures of mitochondrial aspect ratio, area, and density of IMM were completed from all mitochondria that could be traced within the subsarcolemmal space of each image and averaged for each cell. This allowed us to correlate individual measures of mitochondrial behavior and morphology with measures of mitochondrial density and proportion of IMJs from each cell as a whole. We measured a total of 198 mitochondria (90 control, 40 3-hr, and 68 6-hr) from 45 myocytes (three myocytes from each copepod) of 15 copepods (the first five from each treatment group). This sample size of five copepods per group is comparable to other TEM studies (e.g., Leduc-Gaudet et al., 2015; Picard et al., 2013aa). On average, we measured a total of 13 ± 5 mitochondria from each copepod. Only one copepod contained less than eight measured mitochondria (*see* Nielsen et al., 2017).

Mitochondrial density was quantified as the total number of mitochondria in the area (μm^2) of subsarcolemmal space. The proportion of IMJs was calculated as the total number of electron-dense (darker) contact sites divided by the total number of contacts between mitochondria (Picard et al., 2015; *see* Heine and Hood, 2020 *for further explanation of how IMJs are identified*). Mitochondrial area was measured as the size (μm^2) of each mitochondrion by tracing the outer mitochondrial membrane. Mitochondrial aspect ratio was calculated as maximum Feret's diameter divided by minimum Feret's diameter (Marchi et al., 2017), also measured by tracing the outer membrane. Maximum Feret's diameter represents the farthest distance between any two points of the mitochondrion, and minimum Feret's diameter represents the smallest distance between two parallel tangents of the mitochondrion. Density of IMM was quantified using a method adapted from Nielsen et al. (2017). Rows of parallel lines spaced 200 nm apart were overlaid perpendicular to the cristae of each mitochondrion. The total number of intersects between the lines and each crista was divided by the squared area (μm^2) of the mitochondrion. We also recorded the direction of each tissue section determined by the direction of the myofibrils (i.e., longitudinal or transverse).

Before use in the study, the method used to measure density of IMM was validated as follows. For all measured mitochondria from the first copepod of our control group, we quantified the density of IMM using two methods: first, we traced the cristae and divided the total length by the area of the mitochondrion (this gives us a more precise, although time-consuming, estimate of IMM density); second, we used the aforementioned method that estimates the density of IMM using a system of parallel lines. This method was much faster to estimate the density of IMM. Using a general linear regression, we were able to show that a statistically significant, positive linear relationship exists between the two methods (Fig. S1).

The use of TEM to quantify changes in the three-dimensional behavior and morphology of mitochondria has limitations. In particular, the orientation of each muscle cell and mitochondrion when cut in a two-dimensional fashion will—to an extent—impact the values generated in this study. To control for these effects, we oriented and microtomed each copepod in the same manner, included the direction of the myofibrils in each micrograph as a covariate in all behavioral and morphological models, included three cell replicates in our analysis of each copepod, and analyzed all measurable mitochondria from each cell.

2.6. Analytical design

All statistical analyses were completed using R version 3.5.0 (R Core Team, 2018). We used the "lme4" and "lmerTest" libraries for modeling (Bates et al., 2014; Kuznetsova et al., 2017) and the "ggplot2" package (Wickham, 2009) for graphical development.

The metabolic rate of each copepod was modeled using a general linear model (LM) with treatment (control, 3-hr, and 6-hr UV irradiation) as a categorical predictor. Including age as a random effect is synonymous with including mother ID as a random effect, given that each mother produced a clutch of a unique age. The inclusion of age as a random effect in the respiration model did not impact our estimates in any way (*see* R code supplement), therefore, we chose to exclude age as a random effect in our models since all copepods were aged within six days of one another. The effects of UV irradiation on all behavioral and morphological traits were modeled using general linear mixed models (LMMs) with copepod ID retained as a random effect (random intercept) in each model; this allowed us to control for the non-independence of mean estimates among individual copepods since we sampled three myocytes from each individual. The density of IMM and proportion of IMJs were modeled with an interaction between treatment and mitochondrial density, an interaction between treatment and aspect ratio, and section of the tissue as fixed effects. This allowed us to see how mitochondrial density and aspect ratio affect the response variables while also being affected by the UV irradiation treatments themselves. Section was coded as a fixed effect, and not a random effect, since it was comprised of less than five groups (*see* Harrison et al., 2008). Mitochondrial density was also modeled as a response variable since it was not retained in any of the former models after stepwise reduction (*see below*).

Mitochondrial area and mitochondrial density were modeled with treatment and section as fixed effects. Both response variables were cube-root transformed to achieve a normal distribution of model residuals. The cube-root transformation brought the model residuals closer to normality than the square-root transformation for mitochondrial density, and the model residuals were not normally distributed

when mitochondrial area was square-root transformed. Fully-saturated LMMs of mitochondrial behavior and morphology were reduced using the "step" function, but copepod ID was retained as a random effect in all LMMs. Model comparisons were completed using χ^2 analysis, and final models were validated by testing model residuals for normality using the Shapiro-Wilk test.

3. Results

Descriptive statistics of each variable are presented in Table 1.

3.1. Metabolic rate

As an indication of whole-animal performance, we measured the metabolic rate of each copepod following irradiation. As expected, metabolic rate increased with body size in each treatment group (Fig. S2). All copepods survived all irradiation treatments. The metabolic rate of copepods following the 3-hr UV irradiation treatment was maintained with respect to the control treatment (Est. = 0.01; $SE = 0.02$; $p = 0.58$). However, the metabolic rate of copepods exposed to the 6-hr UV irradiation treatment decreased significantly in reference to both the control (Est. = −0.05; $SE = 0.02$; $p = 0.03$) and 3-hr (Est. = −0.06; $SE = 0.02$; $p = 0.006$) treatment groups (Fig. 1).

3.2. Mitochondrial behavior and morphology

To quantify mitochondrial behavior and morphology, we measured several structural components of individual mitochondria (mitochondrial aspect ratio, mitochondrial area, and density of IMM), as well as behavioral aspects of mitochondria within the subsarcolemmal space of the myocyte as a whole (mitochondrial density and proportion of IMJs). We found that the density of IMM increased markedly in both the 3- and 6-hr UV irradiation treatments in comparison to the control group (Fig. 2; Table 2), however, the density of IMM from the 6-hr treatment did not differ significantly from the 3-hr treatment (Est. = 12.03; $SE = 7.21$; $p = 0.12$).

The majority of cristae in mitochondria from the UV-treated groups were exceedingly narrow, and few mitochondria had cristae with intermembrane space that was visible (e.g., Fig. S3). The proportion of IMJs increased significantly with increasing aspect ratio in both UV irradiation treatments (Fig. 3; Table 2), but the proportion of IMJs with increasing aspect ratio did not differ significantly between the 3- and 6-hr treatment groups (Est. = −0.15; $SE = 0.16$; $p = 0.34$). Mitochondrial density increased significantly following both three and six hours of UV irradiation (Fig. 4A; Table 2), however, there was no difference in mitochondrial density of the 6-hr UV irradiation treatment with respect to the 3-hr treatment (Est. = −0.06; $SE = 0.08$; $p = 0.46$). Lastly, mitochondrial size (area) decreased significantly under the 6-hr UV irradiation treatment but not the 3-hr treatment in reference to the control (Fig. 4B; Table 2). The area of mitochondria following six hours of UV irradiation did not differ significantly from the 3-hr treatment group (Est. = −0.01, $SE = 0.04$; $p = 0.73$).

Table 1
Mean estimates, standard deviations, and sample sizes (n) of mitochondrial behavior and morphology traits measured according to UV irradiation treatment.

Variable	n	Control	3-hr UV	6-hr UV
Metabolic rate (mmol O_2 / L / 15 sec / mm body length)	52	0.13 ± 0.09	0.15 ± 0.06	0.08 ± 0.05
Density of IMM (intersects / μm^2)	45	42.1 ± 3.76	69.8 ± 15.7	81.9 ± 18.8
Proportion of IMJs (IMJs / total contacts)	45	0.34 ± 0.30	0.44 ± 0.21	0.49 ± 0.20
Mitochondrial density (mitochondria / μm^2)	45	0.75 ± 0.43	2.13 ± 1.20	1.89 ± 1.01
Mitochondrial area (μm^2)	45	0.47 ± 0.26	0.30 ± 0.24	0.23 ± 0.10
Aspect ratio	45	1.81 ± 0.34	1.98 ± 0.46	2.00 ± 0.65

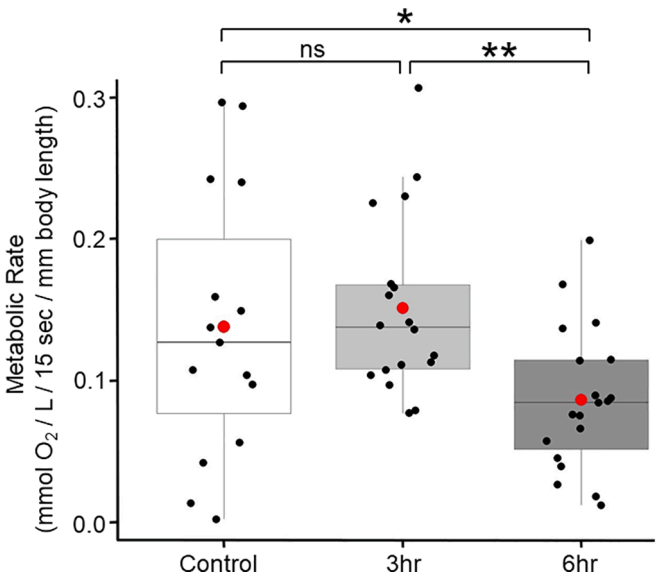

Fig. 1. Effects of UV irradiation on whole-animal metabolic rate. Boxplots showing the effects of UV irradiation on size-adjusted metabolic rates of individual copepods. Large, red dots represent mean estimates. Significance codes: *0.05, **0.01, ns - not significant. (For interpretation of the references to colour in this figure legend, the reader is referred to the web version of this article.)

4. Discussion

Bilaterian animals derive the majority of their energy from oxidative phosphorylation in mitochondria, and much of the research directed toward understanding the role of energy production in animal performance has necessarily focused on the function of the ETS. However, the behavior and morphology of mitochondria can also play key roles in the capacity for energy production. Previous work demonstrated that mitochondrial behavior and morphology influence mitochondrial performance under increased energetic demand, and the literature has also described a large amount of variation that exists in whole-animal performance, both within populations and between taxa (Heine and Hood, 2020). Accordingly, our study aimed to determine how UV radiation influences mitochondrial behavior and morphology at the cellular level, as well as respiratory performance at the organismal level, in myocytes of *Tigriopus californicus* copepods. We hypothesized that UV irradiation induces changes in mitochondrial behavior and morphology, possibly to impact whole-animal metabolic rate under increased energetic demand by increasing the density of IMM and proportion of IMJs.

In copepod myocytes, we found that the density of IMM increased under both three and six hours of UV irradiation, and the proportion of IMJs increased with increasing mitochondrial aspect ratio under UV irradiation. An increase in mitochondrial density and a decrease in mitochondrial size suggest that UV irradiation may induce mitochondrial biogenesis and/or fission. Additionally, copepod metabolic rate was maintained under three hours of UV irradiation but decreased under six hours of exposure. These results indicate that an increase in the density of IMM and proportion of IMJs (along with increased mitochondrial biogenesis and/or fission) may allow animals to maintain their metabolic rate, but this capacity for compensation may be lost at higher levels of UV irradiation. These results have broad implications for understanding variation in whole-animal performance.

Animals must produce enough energy in a cost-effective manner to support survival and reproduction. Recent advances in cell and molecular biology have linked increases in the density of IMM with increased

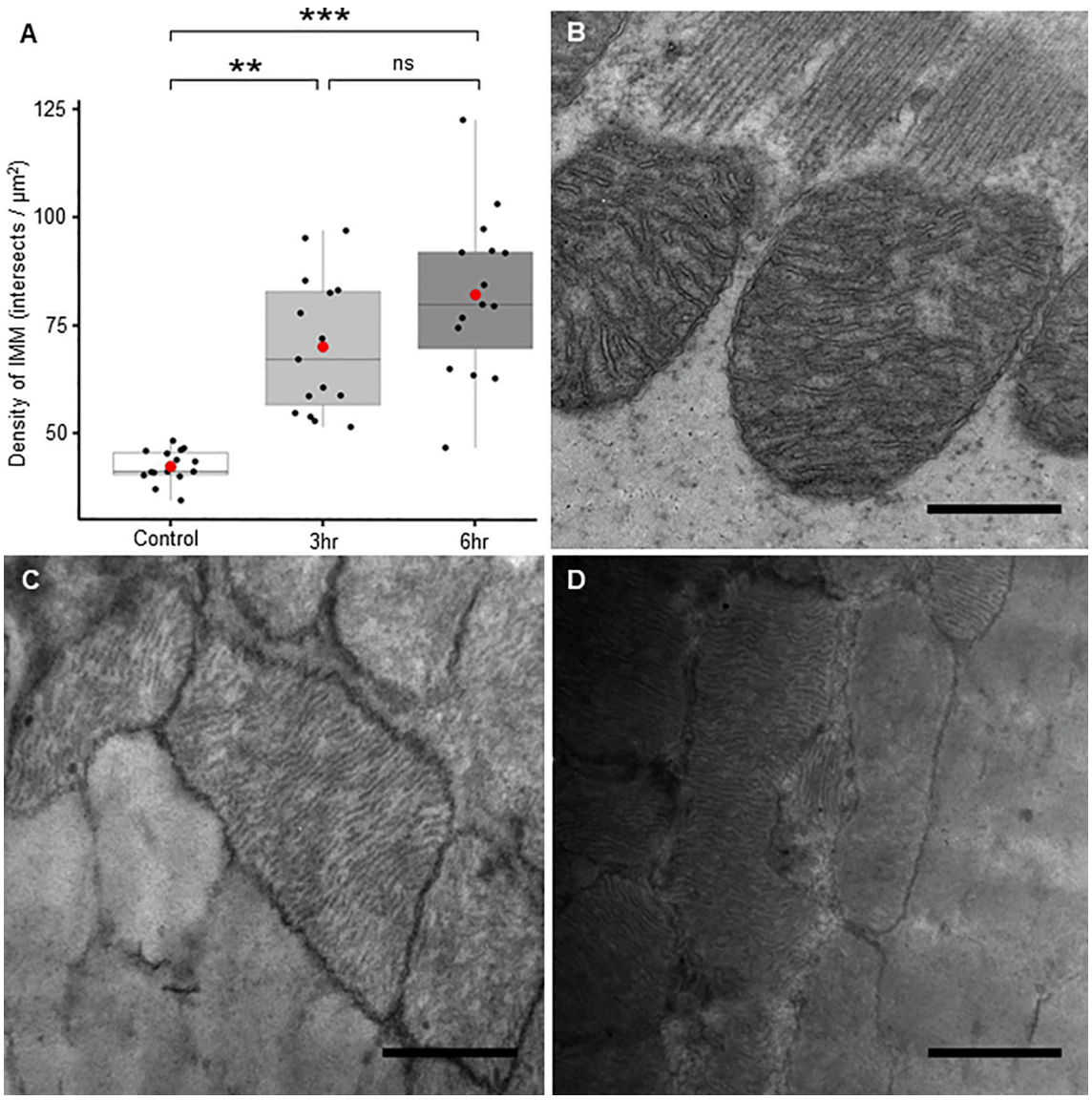

Fig. 2. Effects of UV irradiation on the density of inner mitochondrial membrane. Boxplots showing the (A) effects of UV irradiation on the density of IMM in mitochondria within the subsarcolemmal space of copepod myocytes. Large, red dots represent mean estimates. Significance codes: **0.01, ***0.001, ns - not significant. Transmission electron micrographs show (B) cristae that are wide and distantly spaced from one another within mitochondria from the control treatment, (C) cristae that are narrow and densely packed within mitochondria from the 3-hr UV irradiation treatment, and (D) cristae that are narrow and densely packed within mitochondria from the 6-hr UV irradiation treatment. All scale bars are 500 nm. (For interpretation of the references to colour in this figure legend, the reader is referred to the web version of this article.)

energetic demand (Nielsen et al., 2017), but few studies have evaluated this relationship in an ecological context (e.g., Strohm and Daniels, 2003). As the density of IMM increases within the mitochondrion, the number of protein complexes within the IMM may increase, which could lead to greater (or more efficient) ATP production. Thus, mitochondria can potentially respond to increased demand for energy by increasing the density of cristae, but eventually the quantity of IMM will become so high that cristae can no longer maintain an effective electrochemical gradient (Willis et al., 2016). Accordingly, it is important that we begin to delineate when the IMM should increase in response to environmental stressors and how such an increase impacts animal performance.

UV irradiation can increase the energetic demand of the cell by damaging DNA, lipids, and proteins (Setlow and Setlow, 1962), making energy production within mitochondria less efficient. However, the ROS produced by UV irradiation can act as a cellular signal to upregulate beneficial aspects of mitochondrial behavior such as mitochondrial biogenesis (Zhang et al., 2018), or increase antioxidant production (Han et al., 2016). Such changes have the potential to impact the longevity and reproductive success of the animal as a whole (Heine et al., 2019; Ristow and Schmeisser, 2011; Zhang and Hood, 2016). Consistent with these ideas, we observed that mitochondria increase the density of IMM in response to UV irradiation. While protein markers of biogenesis were not evaluated, an increase in mitochondrial number appears to be a common response to damage that plays a role in rescuing mitochondrial performance (Westermann, 2010). Furthermore, we observed that the respiratory performance of copepods is maintained under lower levels of UV irradiation but decreased under higher levels of UV irradiation. The observed increase in density of the IMM in our study may be the result of mitochondrial repair mechanisms, initiated through mitochondrial fission, that act to discard damaged regions of mitochondria. Consequently, we are left with images of more continuous, intact IMM that are more densely packed into a given area possibly to counteract the damaging effects of UV irradiation. This effort has the potential to fail under higher levels of radiation if efficiency of the mitochondrion

Table 2
Results of LMMs predicting variation in the density of IMM, proportion of IMJs, mitochondrial density, and mitochondrial area. Estimates of mitochondrial density and mitochondrial area are cube-root transformed. Est. is the point estimate, *SE* is the standard error of the estimate, *n* is sample size, and *SD* is the standard deviation of the random effect. Estimates for 3- and 6-hr UV irradiation treatments are in comparison to the control treatment, and transverse sections are in comparison to longitudinal sections. Significance codes: #0.1, *0.05, **0.01, ***0.001, — not retained.

Response	Predictor	*n*	Est. (*SE*)	*SD* (Copepod ID)
Density of IMM				9.26
	3-hr UV	15	27.7 (7.21)**	
	6-hr UV	15	39.7 (7.21)***	
	Mitochondrial density	—	—	
	Aspect Ratio	—	—	
	Transverse	—	—	
Proportion of IMJs				0.04
	3-hr UV	15	−1.00 (0.42)*	
	6-hr UV	15	−0.64 (0.38)	
	Mitochondrial density	—	—	
	Aspect Ratio	45	−0.40 (0.17)*	
	Transverse	—	—	
	3-hr UV : Aspect Ratio	15	0.58 (0.22)*	
	6-hr UV : Aspect Ratio	15	0.43 (0.20)*	
Mitochondrial density				0.09
	3-hr UV	15	0.32 (0.08)**	
	6-hr UV	15	0.26 (0.08)**	
	Transverse	19	0.21 (0.05)***	
Mitochondrial area				0.01
	3-hr UV	15	−0.09 (0.04)#	
	6-hr UV	15	−0.10 (0.04)*	
	Transverse	19	−0.16 (0.03)***	

decreases when the density of IMM becomes too great in comparison to the volume of mitochondrial matrix and surface area of the outer mitochondrial membrane (Mannella, 2006; *see also* Navratil et al., 2008). The lower metabolic rates of copepods in the 6-hr treatment group could be interpreted as beneficial (i.e., they do not need to consume as much oxygen to produce ATP), however, we interpret this decrease in metabolic rate as a detriment, provided that the energetic demand of the cell should increase under increasing UV irradiation. Additionally, Han et al. (2016) has previously shown that the same 3- and 6-hr UV irradiation treatments increase both ROS production and antioxidant enzyme activity in other species of *Tigriopus* copepods. Therefore, a decrease in metabolic rate may indicate greater rates of mitochondrial repair and more efficient metabolism, however, other work has also shown an increase in mortality when metabolic rates decrease following UV irradiation in other copepods (Ma et al., 2013). Further work is needed to determine the extent to which the density of IMM varies with ROS production, oxidative damage, and tissue-specific metabolic rates.

The proportion of IMJs within a cell may facilitate communication between mitochondria and, therefore, the efficiency with which ATP is produced. As such, an increase in energetic demand should be met with more IMJs to upregulate (or maintain) energy production as needed. Since higher levels of UV radiation are known to decrease respiratory performance in copepods (Ma et al., 2013), mitochondria should respond both behaviorally and morphologically to counteract this negative effect. One way that mitochondria can respond to increased energetic demand and/or oxidative stress is to upregulate mitochondrial biogenesis (Zhang et al., 2018), although we found no evidence that the expression of IMJs is linked to mitochondrial density. In both of our UV irradiation treatments, we did observe an increase in the proportion of IMJs in copepod myocytes. However, this increase occurred with increasing aspect ratio of the mitochondria; namely, we observed a greater proportion of IMJs between mitochondria with a lower aspect ratio in our control group, in comparison to more junctions between more elongate mitochondria in our UV-treated groups. If mitochondria became smaller as a result of mitochondrial fission, induced by UV radiation, then elongation is one mechanism by which they could retain a high number of IMJs. Previous work has demonstrated a higher mitochondrial aspect ratio of intermyofibrillar mitochondria than subsarcolemmal mitochondria (Picard et al., 2013b), which may be a product of both the mitochondrion's environment (located between myofibrils versus open space between the myofibrils and cell membrane) or differences in energetic demand at different locations within the cell. Also, previous work in rat soleus muscle has shown significant spreading of mitochondria below the sarcolemma following endurance training (Müller, 1976) and an increase in mitochondrial length in mouse embryonic fibroblasts two to three hours after exposure to UV-C (Tondera et al., 2009). Similarly, our study demonstrates that mitochondria can become more elongate within the subsarcolemmal space of the myocyte, possibly to facilitate communication between mitochondria as energetic demand increases (Heine and Hood, 2020) with increasing oxidative stress (Han et al., 2016). Continuous networks of mitochondria (Kirkwood et al., 1986) within the subsarcolemmal space may also result from the movement of mitochondria towards the intermyofibrillar space (*see* Picard et al., 2013b) or mitochondrial fission.

We found that UV irradiation increased mitochondrial density in both of our UV irradiation treatments but decreased the size of subsarcolemmal mitochondria only in the 6-hr treatment group. An increase in small mitochondria may indicate either an increase in mitochondrial fission or an upregulation of mitochondrial biogenesis (or both; *see* Westermann, 2010; Zhang et al., 2018) within our UV-treated groups. Mitochondrial fission may be an adaptive response to avert apoptosis (Meyer et al., 2017) following an increase in the production of free radicals, and one way to counteract a reduction in mitochondrial size following fission may be to increase mitochondrial biogenesis (Dorn et al., 2015). A decrease in mitochondrial size can result from the cleavage of damaged regions of mitochondria, however, this effect was observed only in the 6-hr UV irradiation group. Therefore, a reduction in size may be merely a byproduct of the fission process but not a direct response to an increase in UV irradiation (i.e., smaller mitochondria are not necessarily more efficient at producing ATP). Previous work in mammalian cell lines has demonstrated instances of stress-induced mitochondrial hyperfusion following UV-C irradiation (Tondera et al., 2009), but the mitochondria in our study showed an increase, not a decrease, in density and were exposed to UV-A/B light. Increasing the number of mitochondria within the cell can increase the overall function of smaller mitochondrial populations as a whole or compensate for the oxidative damage imposed to individual mitochondria. The maintenance of efficient ATP production is likely a delicate balance between mitochondrial biogenesis and fission following an increase in oxidative stress. Overall, an increase in mitochondrial density and/or fission, a greater proportion of IMJs between mitochondria, and a more densely packed IMM within mitochondria, may facilitate more efficient ATP production to counteract the damaging effects of UV irradiation. These processes appear to act concurrently in the myocytes of *T. californicus* copepods but are likely stressor and tissue dependent.

In the wild, *T. californicus* copepods live in shallow splash pools

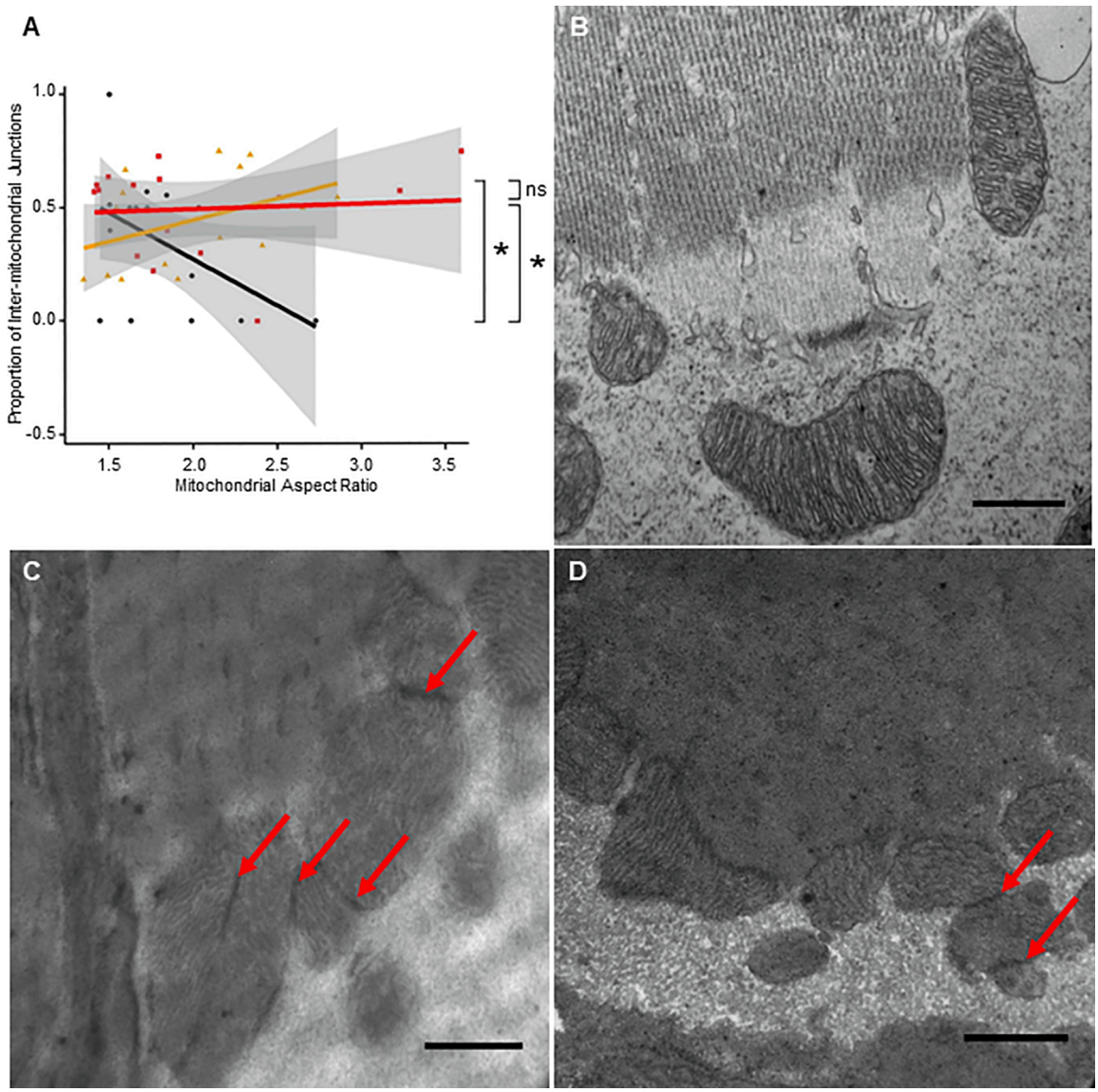

Fig. 3. Effects of UV irradiation on the proportion of inter-mitochondrial junctions. Scatterplot showing the (A) effects of UV irradiation on the proportion of IMJs with increasing aspect ratio between mitochondria within the subsarcolemmal space of copepod myocytes. Gray shading denotes 95% confidence intervals. Black circles, orange triangles, and red squares represent the control, 3-hr, and 6-hr treatment groups, respectively. Significance codes: *0.05, ns - not significant. Transmission electron micrographs show (B) a low proportion of IMJs between elongated mitochondria from the control treatment, (C) a high proportion of IMJs (red arrows) between elongated mitochondria from the 3-hr UV irradiation treatment, and (D) a high proportion of IMJs between elongated mitochondria from the 6-hr UV irradiation treatment. All scale bars are 500 nm. (For interpretation of the references to colour in this figure legend, the reader is referred to the web version of this article.)

above the intertidal zone throughout the west coast of North America (Burton et al., 1979). As with most aquatic organisms, the amount of UV radiation to which copepods are exposed on any given day will vary depending on the taxon and habitat in which they thrive (Overholt et al., 2016). Because they live in shallow pools of water, *T. californicus* copepods are likely exposed to higher levels of radiation than most other species of lake- or ocean-dwelling copepods. Accordingly, our study demonstrates that copepod mitochondria can change their behavior and morphology in response to increasing levels of UV radiation, which may allow them to maintain metabolic rate at lower levels of UV radiation and potentially reduce the costs of maintenance. The same 3-hr UV irradiation treatment in this study was previously shown to increase the reproductive performance of *T. californicus* copepods (Heine et al., 2019). It is plausible that changes in mitochondrial behavior and morphology impact reproductive performance, however, such effects need to be addressed in larger model organisms where the tissue-specific metabolic rates of reproductive tissues can be sampled in conjunction with TEM assays. Also, further work is required to assess the tissue-dependent responses of mitochondria to varying levels of UV radiation in copepods that reside in different environments.

In this study, we demonstrated that UV irradiation can impact whole-animal metabolic rate, possibly through changes in the behavior and morphology of mitochondria. These results illustrate a potential mechanism for how variation in animal function can arise in the face of an exogenous stressor. Additionally, our results show that morphological changes within the cell have the potential to impact metabolic rate even when we do not observe changes in animal function as a whole (i.e., we observed changes in mitochondrial behavior and morphology in the 3-hr UV treatment, but respiratory performance was maintained). Our study suggests that increases in the density of IMM and proportion of IMJs (along with mitochondrial biogenesis and/or fission) in copepod myocytes may allow copepods to maintain metabolic rate under lower levels

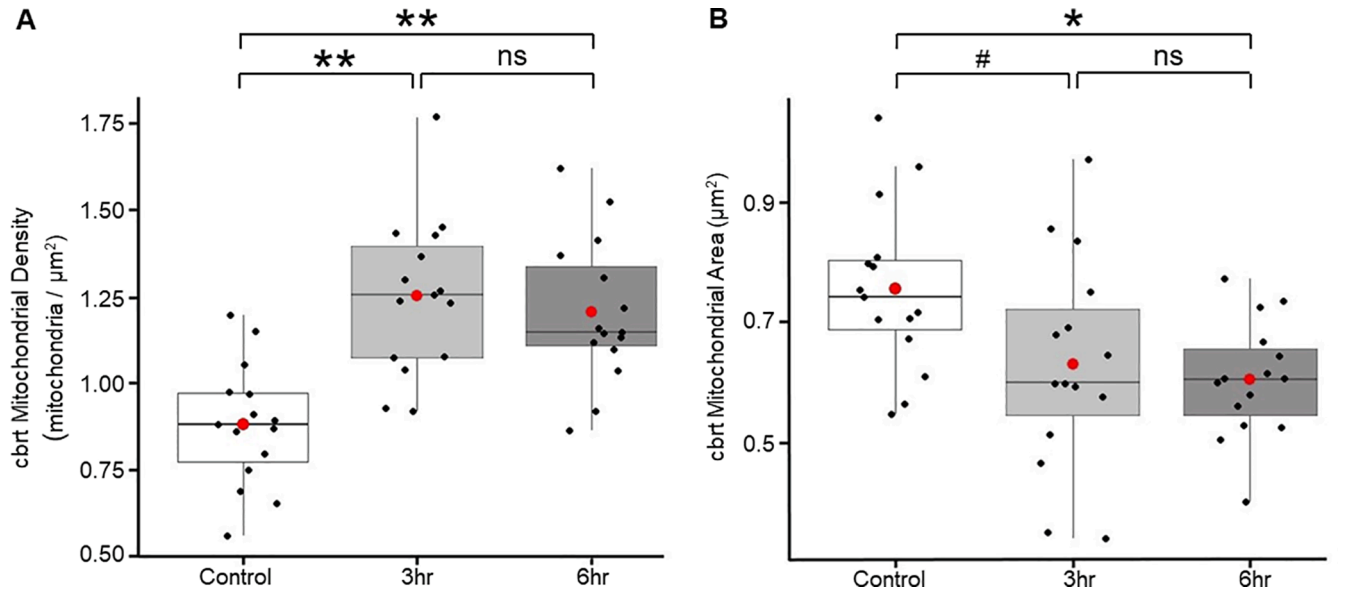

Fig. 4. Effects of UV irradiation on mitochondrial density and area. Boxplots showing the effects of UV irradiation on (A) mitochondrial density and (B) mitochondrial area of mitochondria within the subsarcolemmal space of copepod myocytes. Note the cube-root transformation of both response variables. Large, red dots represent mean estimates. Significance codes: #0.1, *0.05, **0.01, ns - not significant. (For interpretation of the references to colour in this figure legend, the reader is referred to the web version of this article.)

of radiation. Generally, future work on whole-animal performance should continue to address the proximate causes of variation in energy production at the cellular level, as opposed to only characterizing variation of the organism as a whole. By exploring how mitochondrial behavior and morphology respond to energetic challenges and stressors, we will gain a more thorough understanding of how animals support the processes that underlie survival and reproductive success (Heine and Hood, 2020).

5. Data availability

Data and R code are included in the Supplementary material.

Author contributions

K.B.H., G.E.H., and W.R.H. conceived the study; K.B.H. and N.M.J. collected the data; K.B.H. analyzed the data and drafted the manuscript; all authors contributed to editing the manuscript and are accountable for all work published herein.

Funding

This work was supported by National Science Foundation grants IOS1453784 and OIA1736150. K.B.H. was supported by a graduate research fellowship from the American Microscopical Society.

Declaration of Competing Interest

The authors declare that they have no known competing financial interests or personal relationships that could have appeared to influence the work reported in this paper.

Acknowledgments

We would like to thank Matt Powers for assistance with respiration assays and the Auburn University Research Instrumentation Facility for access to microtoming and TEM equipment. We also thank the Hill and Hood laboratory groups for comments on an early version of the manuscript, as well as Daniel Jung, Ben Pollock, and Victoria Tucker for assistance with copepod husbandry.

Appendix A. Supplementary data

Supplementary data to this article can be found online at https://doi.org/10.1016/j.mito.2020.11.001.

References

Bates, D., Mächler, M., Bolker, B. and Walker, S., 2014. Fitting linear mixed-effects models using lme4. arXiv:1406.5823.

Burton, R.S., 1985. Mating system of the intertidal copepod *Tigriopus californicus*. Mar. Biol. 86, 247–252. https://doi.org/10.1007/BF00397511.

Burton, R.S., Feldman, M.W., Curtsinger, J.W., 1979. Population genetics of *Tigriopus californicus* (Copepoda: Harpacticoida): I. Population structure along the central California coast. Marine Ecol. Prog. Ser. 1, 29–39.

Cadet, J., Sage, E., Douki, T., 2005. Ultraviolet radiation-mediated damage to cellular DNA. Mutation Research/Fundam. Mol. Mech. Mutagenesis 571, 3–17. https://doi.org/10.1016/j.mrfmmm.2004.09.012.

Dorn II, G.W., Vega, R.B., Kelly, D.P., 2015. Mitochondrial biogenesis and dynamics in the developing and diseased heart. Genes Dev. 29, 1981–1991. https://doi.org/10.1101/gad.269894.115.

Drent, R.H., Daan, S., 1980. The prudent parent: energetic adjustments in avian breeding. Ardea 68, 225–252. https://doi.org/10.5253/arde.v68.p225.

Finkel, T., Holbrook, N.J., 2000. Oxidants, oxidative stress and the biology of ageing. Nature 408, 239–247. https://doi.org/10.1038/35041687.

Han, J., Puthumana, J., Lee, M.C., Kim, S., Lee, J.S., 2016. Different susceptibilities of the Antarctic and temperate copepods *Tigriopus kingsejongensis* and *T. japonicus* to ultraviolet (UV) radiation. Mar. Ecol. Prog. Ser. 561, 99–107. https://doi.org/10.3354/meps11946.

Harrison, X.A., Donaldson, L., Correa-Cano, M.E., Evans, J., Fisher, D.N., Goodwin, C.E., Robinson, B.S., Hodgson, D.J., Inger, R., 2008. A brief introduction to mixed effects modelling and multi-model inference in ecology. PeerJ 6. https://doi.org/10.7717/peerj.4794 e4794.

Hatefi, Y., 1985. The mitochondrial electron transport and oxidative phosphorylation system. Annu. Rev. Biochem. 54, 1015–1069. https://doi.org/10.1146/annurev.bi.54.070185.005055.

Heck, D.E., Vetrano, A.M., Mariano, T.M., Laskin, J.D., 2003. UVB light stimulates production of reactive oxygen species unexpected role for catalase. J. Biol. Chem. 278, 22432–22436. https://doi.org/10.1074/jbc.C300048200.

Heine, K.B., Hood, W.R., 2020. Mitochondrial behaviour, morphology, and animal performance. Biol. Rev. 95, 730–737. https://doi.org/10.1111/brv.12584.

Heine, K.B., Powers, M.J., Kallenberg, C., Tucker, V.L., Hood, W.R., 2019. Ultraviolet irradiation increases size of the first clutch but decreases longevity in a marine copepod. Ecol. Evol. 9, 9759–9767. https://doi.org/10.1002/ece3.5510.

Hill, G.E., 2019. Mitonuclear Ecology. Oxford University Press, Oxford, UK.

Hood, W.R., Zhang, Y., Mowry, A.V., Hyatt, H.W., Kavazis, A.N., 2018. Life history trade-offs within the context of mitochondrial hormesis. Integr. Comp. Biol. 58, 567–577. https://doi.org/10.1093/icb/icy073.

Hood, W.R., Zhang, Y., Taylor, H.A., Park, N.R., Beatty, A.E., Weaver, R.J., Yap, K.N., Kavazis, A.N., 2019. Prior reproduction alters how mitochondria respond to an oxidative event. J. Exp. Biol. 222, jeb195545. https://doi.org/10.1242/jeb.195545.
Hopkins, C.C.E., 1978. The male genital system, and spermatophore production and function in *Euchaeta norvegica* Boeck (Copepoda: Calanoida). J. Exp. Mar. Biol. Ecol. 35, 197–231. https://doi.org/10.1016/0022-0981(78)90076-X.
Hylander, S., Grenvald, J.C., Kiørboe, T., Pfrender, M., 2014. Fitness costs and benefits of ultraviolet radiation exposure in marine pelagic copepods. Funct. Ecol. 28, 149–158. https://doi.org/10.1111/1365-2435.12159.
Kenagy, G.J., Masman, D., Sharbaugh, S.M., Nagy, K.A., 1990. Energy expenditure during lactation in relation to litter size in free-living golden-mantled ground squirrels. J. Anim. Ecol. 59, 73. https://doi.org/10.2307/5159.
Kirkwood, S.P., Munn, E.A., Brooks, G.A., 1986. Mitochondrial reticulum in limb skeletal muscle. Am. J. Physiol.-Cell Physiol. 251, C395–C402. https://doi.org/10.1152/ajpcell.1986.251.3.C395.
Kuznetsova, A., Brockhoff, P.B., Christensen, R.H.B., 2017. lmerTest package: tests in linear mixed effects models. J. Stat. Softw. 82, 1–26. https://doi.org/10.18637/jss.v082.i13.
Leduc-Gaudet, J.-P., Picard, M., Pelletier, F.-J., Sgarioto, N., Auger, M.-J., Vallée, J., Robitaille, R., St-Pierre, D.H., Gouspillou, G., 2015. Mitochondrial morphology is altered in atrophied skeletal muscle of aged mice. Oncotarget 6, 17923–17937. https://doi.org/10.18632/oncotarget.4235.
Ma, Z., Li, W., Gao, K., 2013. Impacts of UV radiation on respiration, ammonia excretion, and survival of copepods with different feeding habits. Hydrobiologia 701, 209–218. https://doi.org/10.1007/s10750-012-1275-x.
Mannella, C.A., 2006. The relevance of mitochondrial membrane topology to mitochondrial function. Biochim. Biophys. Acta (BBA) – Mol. Basis Dis. 1762, 140–147. https://doi.org/10.1016/j.bbadis.2005.07.001.
Mannella, C.A., Lederer, W.J., Jafri, M.S., 2013. The connection between inner membrane topology and mitochondrial function. J. Mol. Cell. Cardiol. 62, 51–57. https://doi.org/10.1016/j.yjmcc.2013.05.001.
Marchi, S., Bonora, M., Patergnani, S., Giorgi, C., Pinton, P., 2017. Methods to assess mitochondrial morphology in mammalian cells mounting autophagic or mitophagic responses. In: Methods in Enzymology. Academic Press, pp. 171–186. https://doi.org/10.1016/bs.mie.2016.09.080.
Meyer, J.N., Leuthner, T.C., Luz, A.L., 2017. Mitochondrial fusion, fission, and mitochondrial toxicity. Toxicology 391, 42–53. https://doi.org/10.1016/j.tox.2017.07.019.
Müller, W., 1976. Subsarcolemmal mitochondria and capillarization of soleus muscle fibers in young rats subjected to an endurance training. Cell Tissue Res. 174, 367–389. https://doi.org/10.1007/BF00220682.
Navratil, M., Terman, A., Arriaga, E.A., 2008. Giant mitochondria do not fuse and exchange their contents with normal mitochondria. Exp. Cell Res. 314, 164–172. https://doi.org/10.1016/j.yexcr.2007.09.013.
Ng, W.-L., Bassler, B.L., 2009. Bacterial quorum-sensing network architectures. Annu. Rev. Genet. 43, 197–222. https://doi.org/10.1146/annurev-genet-102108-134304.
Nielsen, J., Gejl, K.D., Hey-Mogensen, M., Holmberg, H.-C., Suetta, C., Krustrup, P., Elemans, C.P.H., Ørtenblad, N., 2017. Plasticity in mitochondrial cristae density allows metabolic capacity modulation in human skeletal muscle: enlarged mitochondrial cristae density in athletes. J Physiol 595, 2839–2847. https://doi.org/10.1113/JP273040.
Overholt, E.P., Rose, K.C., Williamson, C.E., Fischer, J.M., Cabrol, N.A., 2016. Behavioral responses of freshwater calanoid copepods to the presence of ultraviolet radiation: avoidance and attraction. J. Plankton Res. 38, 16–26. https://doi.org/10.1093/plank t/fbv113.
Pacher, P., Hajnoczky, G., 2001. Propagation of the apoptotic signal by mitochondrial waves. EMBO J. 20, 4107–4121. https://doi.org/10.1093/emboj/20.15.4107.
Picard, M., Gentil, B.J., McManus, M.J., White, K., St. Louis, K., Gartside, S.E., Wallace, D.C., Turnbull, D.M., 2013a. Acute exercise remodels mitochondrial membrane interactions in mouse skeletal muscle. J. Appl. Physiol. 115, 1562–1571. https://doi.org/10.1152/japplphysiol.00819.2013.
Picard, M., White, K., Turnbull, D.M., 2013b. Mitochondrial morphology, topology, and membrane interactions in skeletal muscle: a quantitative three-dimensional electron microscopy study. J. Appl. Physiol. 114, 161–171. https://doi.org/10.1152/japplphysiol.01096.2012.
Picard, M., McManus, M.J., Csordás, G., Várnai, P., Dorn II, G.W., Williams, D., Hajnóczky, G., Wallace, D.C., 2015. Trans-mitochondrial coordination of cristae at regulated membrane junctions. Nat. Commun. 6, 6259. https://doi.org/10.1038/ncomms7259.
R Core Team, 2018. R: A language and environment for statistical computing. Vienna, Austria: R Foundation for Statistical Computing. http://www.R-project:.
Ristow, M., Schmeisser, S., 2011. Extending life span by increasing oxidative stress. Free Radical Biol. Med. 51, 327–336. https://doi.org/10.1016/j.freeradbiomed.2011.05.010.
Rueden, C.T., Schindelin, J., Hiner, M.C., DeZonia, B.E., Walter, A.E., Arena, E.T., Eliceiri, K.W., 2017. ImageJ2: ImageJ for the next generation of scientific image data. BMC Bioinf. 18 https://doi.org/10.1186/s12859-017-1934-z.
Salin, K., Villasevil, E.M., Anderson, G.J., Lamarre, S.G., Melanson, C.A., McCarthy, I., Selman, C., Metcalfe, N.B., 2019. Differences in mitochondrial efficiency explain individual variation in growth performance. Proc. R. Soc. B. 286, 20191466. https://doi.org/10.1098/rspb.2019.1466.
Santo-Domingo, J., Giacomello, M., Poburko, D., Scorrano, L., Demaurex, N., 2013. OPA1 promotes pH flashes that spread between contiguous mitochondria without matrix protein exchange. EMBO J. 32, 1927–1940. https://doi.org/10.1038/emboj.2013.124.
Setlow, R.B., Setlow, J.K., 1962. Evidence that ultraviolet-induced thymine dimers in DNA cause biological damage. Proc. Natl. Acad. Sci. 48, 1250–1257. https://doi.org/10.1073/pnas.48.7.1250.
Speakman, J.R., Blount, J.D., Bronikowski, A.M., Buffenstein, R., Isaksson, C., Kirkwood, T.B.L., Monaghan, P., Ozanne, S.E., Beaulieu, M., Briga, M., Carr, S.K., Christensen, L.L., Cochemé, H.M., Cram, D.L., Dantzer, B., Harper, J.M., Jurk, D., King, A., Noguera, J.C., Salin, K., Sild, E., Simons, M.J.P., Smith, S., Stier, A., Tobler, M., Vitikainen, E., Peaker, M., Selman, C., 2015. Oxidative stress and life histories: unresolved issues and current needs. Ecol. Evol. 5, 5745–5757. https://doi.org/10.1002/ece3.1790.
Speakman, J.R., Król, E., 2005. Limits to sustained energy intake IX: a review of hypotheses. J. Comp. Physiol. B 175, 375–394. https://doi.org/10.1007/s00360-005-0013-3.
Strohm, E., Daniels, W., 2003. Ultrastructure meets reproductive success: performance of a sphecid wasp is correlated with the fine structure of the flight–muscle mitochondria. Proc. R. Soc. Lond. B 270, 749–754. https://doi.org/10.1098/rspb.2002.2282.
Tondera, D., Grandemange, S., Jourdain, A., Karbowski, M., Mattenberger, Y., Herzig, S., Da Cruz, S., Clerc, P., Raschke, I., Merkwirth, C., Ehses, S., Krause, F., Chan, D.C., Alexander, C., Bauer, C., Youle, R., Langer, T., Martinou, J.-C., 2009. SLP-2 is required for stress-induced mitochondrial hyperfusion. EMBO J. 28, 1589–1600. https://doi.org/10.1038/emboj.2009.89.
Weaver, R.J., Wang, P., Hill, G.E., Cobine, P.A., 2018. An in vivo test of the biologically relevant roles of carotenoids as antioxidants in animals. J. Exp. Biol. 221, jeb183665. https://doi.org/10.1242/jeb.183665.
Westermann, B., 2010. Mitochondrial fusion and fission in cell life and death. Nat. Rev. Mol. Cell Biol. 11, 872–884. https://doi.org/10.1038/nrm3013.
Wickham, H., 2009. ggplot2: Elegant graphics for data analysis. Springer New York, New York, NY.
Willis, W.T., Jackman, M.R., Messer, J.I., Kuzmiak-Glancy, S., Glancy, B., 2016. A simple hydraulic analog model of oxidative phosphorylation. Med. Sci. Sports Exerc. 48, 990–1000. https://doi.org/10.1249/MSS.0000000000000884.
Zhang, Y., Hood, W.R., 2016. Current versus future reproduction and longevity: a re-evaluation of predictions and mechanisms. J. Exp. Biol. 219, 3177–3189. https://doi.org/10.1242/jeb.132183.
Zhang, Y., Humes, F., Almond, G., Kavazis, A.N., Hood, W.R., 2018. A mitohormetic response to pro-oxidant exposure in the house mouse. Am. J. Physiol.-Regul., Integr. Comparat. Physiol. 314, 122–134. https://doi.org/10.1152/ajpregu.00176.2017.
Zick, M., Rabl, R., Reichert, A.S., 2009. Cristae formation—linking ultrastructure and function of mitochondria. Biochim. Biophys. Acta 1793, 5–19. https://doi.org/10.1016/j.bbamcr.2008.06.013.